A crossover in anisotropic nanomechanochemistry of van der Waals crystals

Kohei Shimamura, Masaaki Misawa, Ying Li, Rajiv K. Kalia, Aiichiro Nakano, Fuyuki Shimojo, and Priya Vashishta

Citation: Applied Physics Letters **107**, 231903 (2015); doi: 10.1063/1.4937268
View online: http://dx.doi.org/10.1063/1.4937268
View Table of Contents: http://scitation.aip.org/content/aip/journal/apl/107/23?ver=pdfcov
Published by the AIP Publishing

A crossover in anisotropic nanomechanochemistry of van der Waals crystals

Kohei Shimamura,[1,2,3] Masaaki Misawa,[1,2] Ying Li,[4] Rajiv K. Kalia,[2] Aiichiro Nakano,[2] Fuyuki Shimojo,[1] and Priya Vashishta[2]
[1]*Department of Physics, Kumamoto University, Kumamoto 860-8555, Japan*
[2]*Collaboratory for Advanced Computing and Simulations, Department of Physics and Astronomy, Department of Computer Science, Department of Chemical Engineering and Materials Science, University of Southern California, Los Angeles, California 90089-0242, USA*
[3]*Graduate School of System Informatics, Kobe University, Kobe 657-8501, Japan*
[4]*Argonne Leadership Computing Facility, Argonne National Laboratory, Argonne, Illinois 60439, USA*

(Received 14 June 2015; accepted 24 November 2015; published online 8 December 2015)

In nanoscale mechanochemistry, mechanical forces selectively break covalent bonds to essentially control chemical reactions. An archetype is anisotropic detonation of layered energetic molecular crystals bonded by van der Waals (vdW) interactions. Here, quantum molecular dynamics simulations reveal a crossover of anisotropic nanomechanochemistry of vdW crystal. Within 10^{-13} s from the passage of shock front, lateral collision produces NO_2 via twisting and bending of nitro-groups and the resulting inverse Jahn-Teller effect, which is mediated by strong *intra-layer* hydrogen bonds. Subsequently, as we transition from heterogeneous to homogeneous mechanochemical regimes around 10^{-12} s, shock normal to multilayers becomes more reactive, producing H_2O assisted by *inter-layer* N-N bond formation. These time-resolved results provide much needed atomistic understanding of nanomechanochemistry that underlies a wider range of technologies.
 [http://dx.doi.org/10.1063/1.4937268]

Recent advances in experimental techniques have raised the exciting possibility to rationally design materials, in which chemical reactions are controlled mechanically.[1–3] Such mechanochemistry can now be studied dynamically at the nanoscale with recently developed nanoreactors[4] and nanoscale impact experiments.[5] In nanomechanochemistry, mechanical forces selectively break covalent bonds. A prime example is the detonation of energetic materials, where a mechanical shock wave initiates exothermic reactions to self-sustain wave propagation.[6,7] In typical energetic molecular crystals, it takes only 10^{-13} s (i.e., the period of one molecular vibration) for a detonation wave front to pass through each molecule. This time scale is too short for chemical reactions to be thermally activated. Consequently, reactions are likely initiated athermally via mechanical activation.[8] (While this is concerned with the initiation of reactions, their completion takes much longer time.) An archetypal nanomechanochemistry occurs in triaminotrinitrobenzene (TATB). It was suggested theoretically that mechanical bending of a nitrate group in a TATB molecule closes the energy gap between the highest occupied molecular orbital (HOMO) and the lowest unoccupied molecular orbital (LUMO) through an inverse Jahn-Teller effect.[8,9] The closing of the HOMO-LUMO gap liberates bonding electrons to initiate chemical reactions. But this was a single-molecule calculation and did not address mechanochemistry in solid.

TATB belongs to a broad class of layered molecular crystals that are bonded by inter-layer van der Waals (vdW) interactions,[10–13] similar to vdW materials that are gaining growing attention due to their unique physical and chemical properties.[14,15] Within each layer, on the other hand, these crystals are inter-bonded by a strong hydrogen-bond network in addition to intra-molecular covalent bonds. Interplay between the inter-layer vdW and intra-layer hydrogen bonds is expected to dictate anisotropic detonation behaviors of these energetic vdW crystals. This is akin to other polar vdW crystals that exhibit peculiar behaviors.[16] A fundamental scientific question is thus: How does the interplay of vdW and hydrogen bonds determine anisotropic nanomechanochemistry in vdW crystals at different time scales? Recent nanoscale impact experiments have studied mechanical responses of multilayer vdW materials,[5] and similar mechanochemical anisotropy was studied previously using binary collision of pentaerythritol tetranitrate (PETN) molecules.[17,18] However, such bi-molecular collision cannot capture the inter-layer/intra-layer effects of interest.

To address this key issue, we have recently introduced "*ab initio* nanocollider" simulation, in which the collision of two TATB crystallites was studied using quantum molecular dynamics (QMD) simulations in the framework of density functional theory (DFT).[19] QMD follows the trajectories of all atoms while computing interatomic interactions quantum mechanically. Our nanocollider simulations revealed atomistic mechanisms of anisotropic shock sensitivity.[20] Highly sensitive lateral collision was found to originate from the twisting and bending of nitro-groups mediated by strong intra-layer hydrogen bonds. This causes the closing of the electronic energy gap due to an inverse Jahn-Teller effect. On the other hand, insensitive collision normal to multilayers is accompanied by more delocalized molecular deformations mediated by inter-layer interaction. Figure S1 in the supplementary material demonstrates highly heterogeneous deformations at the shock front, i.e., different molecules undergo drastically different deformations, hence heterogeneous mechanochemistry.[19] Figures S2(a) and S2(b) show massive

NO_2 production in lateral collision as well as the absence of such reaction in normal collision.[19] The anisotropic mechanochemical responses resulted in much higher temperature during lateral collision (Fig. S2(c)) than that during normal collision (Fig. S2(d)).[19]

These nanocollider simulations atomistically studied chemical reactions at the heterogeneous unshocked-shocked material interface. Namely, they probed short-time heterogeneous nanomechanochemistry occurring at the time scales of 10^{-13} s or equivalently in the first molecular layer at the shock front. For nanocollider study at a longer time scale τ, proportionally longer $O(\tau)$ system length is required in the shock direction. Combined with the N^3 computational complexity of DFT (N is the number of atoms), the resulting computational cost scales as $O(\tau^6)$, making *ab initio* nanocollider simulations of longer time scales prohibitive.

At longer time scales (~beyond 10^{-12} s), the multiscale shock technique (MSST) developed by Reed *et al*. follows homogeneous reaction pathways (i.e., molecular deformations are uniform across crystalline unit cells) subject to macroscopic conservation laws of the mass, momentum, and energy.[7,21] Namely, MSST probes long-time *homogeneous* thermochemistry in contrast to short-time *heterogeneous* mechanochemistry in nanocollider (Fig. S3).[19] A similar method was utilized in the recent nanoreactor study[4] of thermochemistry. Here, we perform MSST simulations to study thermochemical reaction pathways in shocked TATB crystal in contrast to mechanochemical reaction pathways in our previous nanocollider simulations at shorter time scales.

TATB is a rather insensitive aromatic explosive, based on the basic six-carbon benzene ring structure with three nitro functional groups (NO_2) and three amine (NH_2) groups attached, alternating around the ring.[22–24] The simulated triclinic supercell contains 8 TATB molecules (in total of 192 atoms) and has the lattice parameters: $a = 9.013$ Å, $b = 18.417$ Å, $c = 13.624$ Å, $\alpha = 108.58°$, $\beta = 91.82°$, and $\gamma = 119.97°$ (Fig. 1). The lattice parameters were determined such that axial stresses (P_{xx}, P_{yy}, and P_{zz}) became zero when performing structural optimization. Periodic boundary conditions were applied in all directions.

Two MSST simulations were performed,[19] in which shock waves propagated in the crystallographic b and c directions, respectively, with a shock speed of 10 km/s. Initial temperature was set to 300 K. The equations of motion were integrated numerically with a time step of 0.242 fs. Simulations were performed for the time duration of 1.21 ps.

Thermomechanical response: Figure 2 shows the temperature (T), pressure (P), volume ratio (V/V_0 with V_0 being the initial volume), and particle velocity (v_p) as a function of time t for shock propagation in b and c directions. Temporal response of these quantities to shock in the figure exhibits significant crystallographic anisotropy. For all the four quantities, there is rapid change around 100 fs in c direction. On the other hand, a similar change occurs at later time (only after 300 fs) in b direction. Also notable is the oscillation of P, V/V_0, and v_p with a period of ~100 fs in c direction. This is understandable as a result of multiple collisions of TATB layers that are only weakly bonded by vdW interaction in c direction (Fig. 1).

Despite the different response times, the pressure, volume, and particle velocity in b and c directions converge to the almost identical values within 1 ps. The values of P and V/V_0 for c direction are nearly identical with those by Manaa *et al*. in the same time scale,[22] though they used a more approximate density-functional tight binding (DFTB) method to simulate longer time scales. In contrast, the temperature is different between b and c directions even at the end of the simulations. The temperature in b direction rapidly increases at around 300 fs, and subsequently it gradually increases from around 1800 to 2500 K. On the other hand, T in c direction rapidly increases at around 100 fs and then gradually increases from 2000 to 3000 K. This indicates more extensive exothermic reactions in c direction than in b direction. However, it shoud be noted that much longer time is required before T reaches the asymptotic value. According to the previous simulations on TATB[22] and related energetic molecular crystals,[25] this will take longer than ns. Supplementary movies show the atomic trajectories of the MSST simulations of b-axis and c-axis shock, respectively.[19] Figure S4 shows the nonequilibrium nature of the thermodynamic states.[19]

Anisotropic reaction dynamics: In order to understand the nature of anisotropic reactions, we performed bond-overlap population (BOP) analysis.[19] Figures 3(a) and 3(b) show snapshots of part of atomic configurations in b-axis and c-axis shock, respectively. The corresponding time

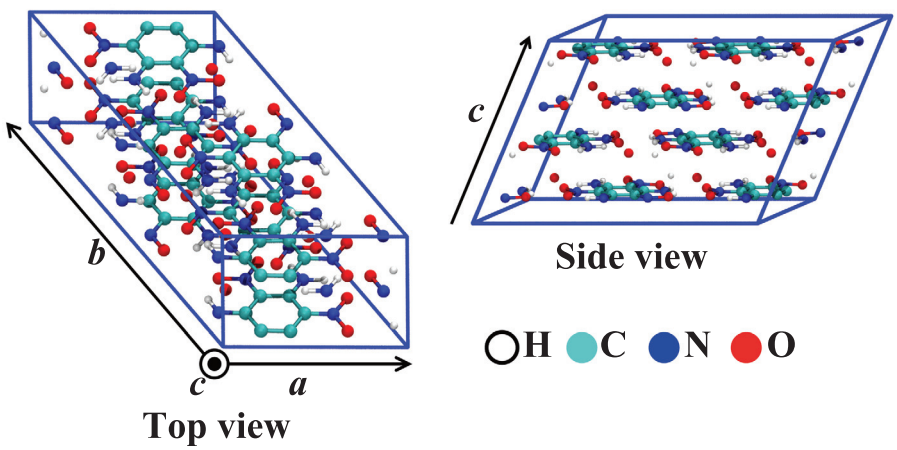

FIG. 1. Simulated TATB crystals. The atomic configuration after structural optimization is shown, where white, cyan, blue, and red spheres represent H, C, N, and O atoms, respectively. The left and right panels show configurations for b-axis and c-axis shock simulations, respectively.

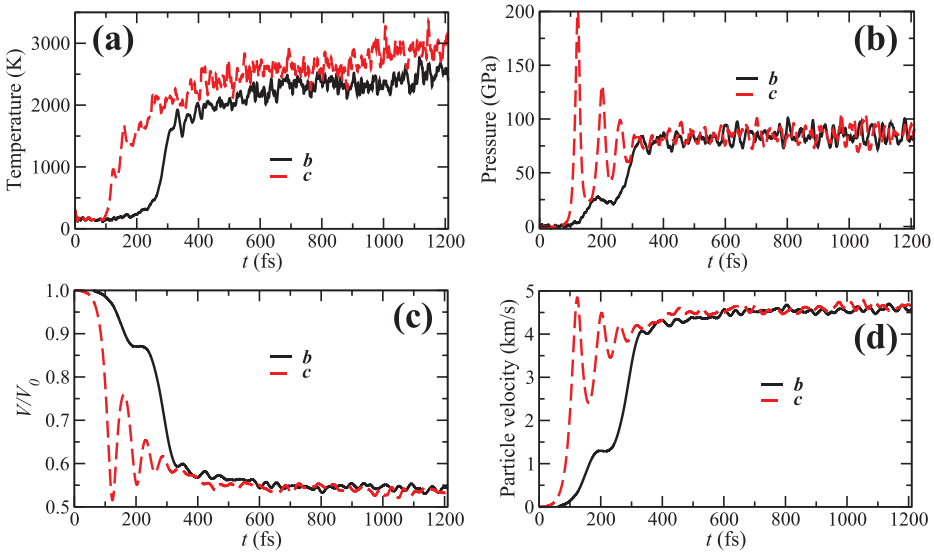

FIG. 2. Anisotropic thermomechanical response to shock. Time evolution of the temperature (a), pressure (b), volume (c), and particle velocity (d) for shock propagation in *b* (solid black lines) and *c* (dashed red lines) directions.

evolution of BOPs, $O_{ij}(t)$, between key pairs of atoms, *i*-*j*, involved in reactions is shown in Figs. 3(c) and 3(d), respectively, for *b*-axis and *c*-axis shock. As shown in Fig. 3(c) for *b*-axis shock, initial bond strengths between O1-H1 and O2-H2 are small. However, the bonds suddenly strengthen beyond that of hydrogen bonding at 177 fs. This is likely due to the increase of pressure, i.e., the narrowing of intermolecular distances. Further increase of pressure is released by the bending of NO_2 and NH_2 groups at 281 fs, leading to the destruction of the layer structure at 358 fs. It should be noted that the stress-release mechanism is not the same at other intermolecular contacts. Namely, we also observed twisting of NO_2 and NH_2 groups. Geometry of the intermolecular contacts is highly irregular in *b*-axis shock.

In marked contrast, intermolecular contacts in *c*-axis shock are highly ordered. Since multiple layers are bonded only by weak vdW interaction, intermolecular bonds along the shock direction are very weak. As a consequence, molecules from neighboring layers repeatedly collide in an elastic-collision manner. This is reflected in oscillation of period ∼100 fs in Fig. 2 in the first 300 fs. Here, atoms from neighboring layers that are positioned on top of each other along the *c* axis become targets of repeated collisions. Examples are N1-N4, N2-N3, C2-O5, and C4-O4 in Fig. 3(b). At 121 fs, these atoms approach each other significantly by shock, and antibonds are formed between these pairs as shown by negative BOP values in Fig. 3(d). Shortly after that, BOPs of N1-N4 and N2-N3 become positive, indicating the formation of bonding states. Formation of these N-N bonds in turn leads to the dissociation of H and O atoms from the N atoms. As shown in the snapshot at 182 fs in Fig. 3(b), N2 and N4 release H3 and H4, respectively, whereas

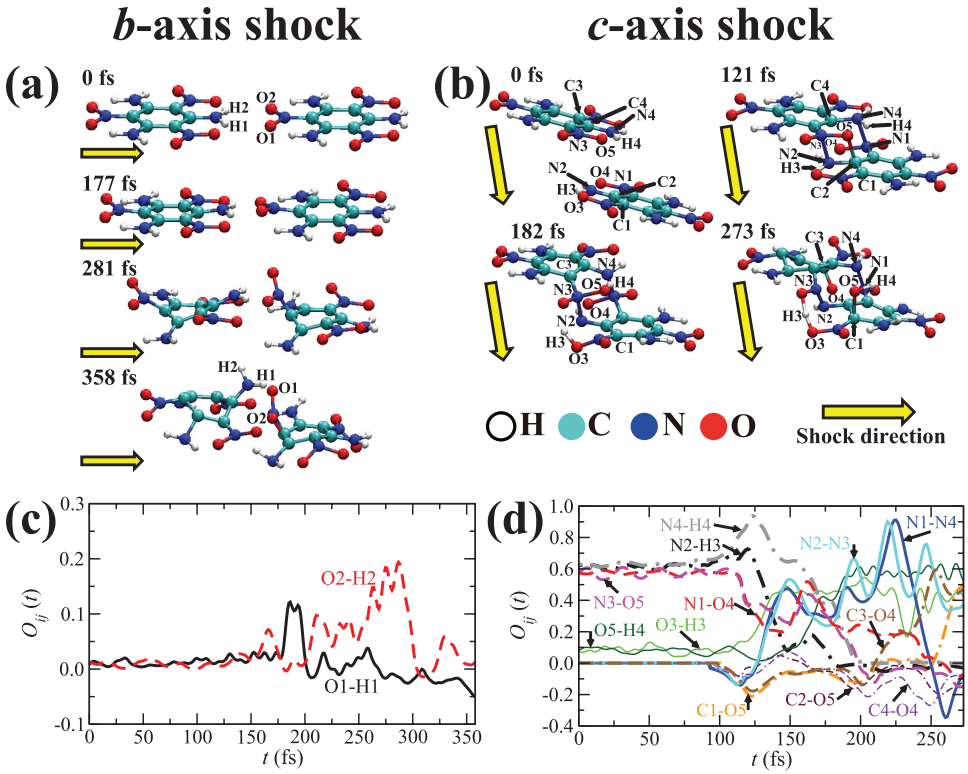

FIG. 3. Anisotropic reaction dynamics. Snapshots of part of atomic configurations in *b*-axis (a) and *c*-axis (b) shock, where numerals show indices of key atoms involved in reactions. Time evolution of BOPs $O_{ij}(t)$ between selected atoms in *b*-axis (c) and *c*-axis (d) shock.

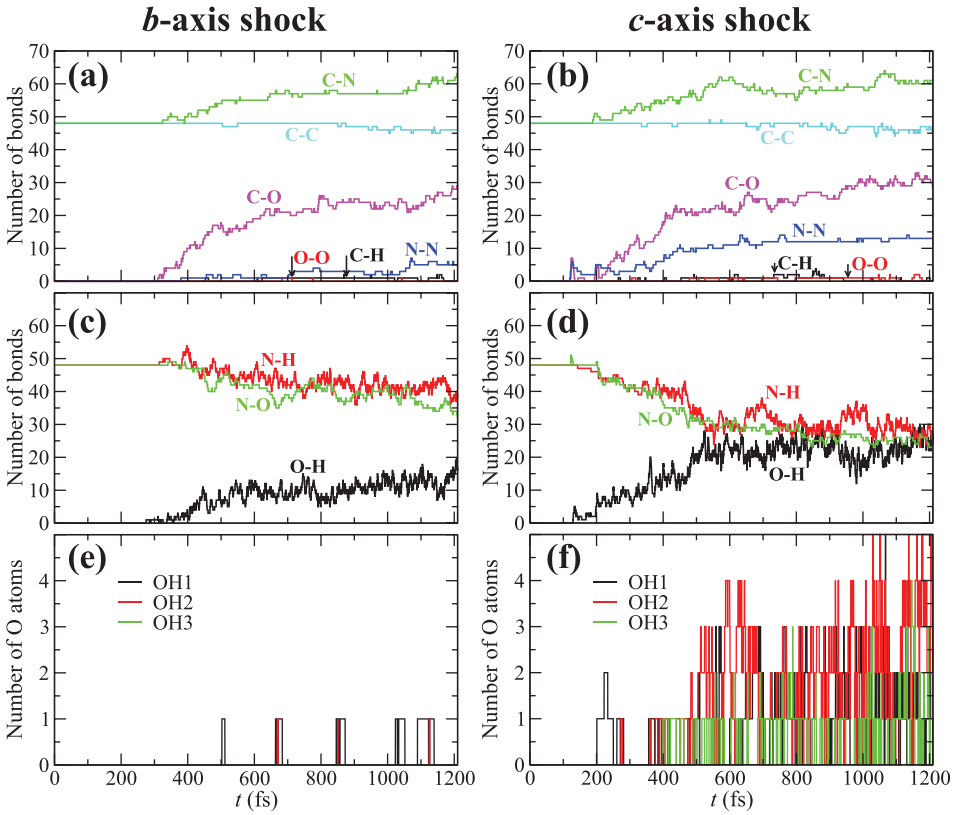

FIG. 4. Anisotropic bond dynamics. Time evolution of the number of C-H, C-C, C-N, C-O, N-H, N-N, N-O, O-H, and O-O bonds in *b*-axis shock ((a) and (c)) and *c*-axis shock ((b) and (d)), respectively. Time evolution of the number of O atoms that are bonded to one (OH1), two (OH2), and three (OH3) H atoms in *b*-axis (e) and *c*-axis (f) shock, respectively.

O4 and O5 are released from N1 and N3 at 273 fs. The reason why the N1-N4 bond becomes antibonding at around 250 fs is that these N atoms bond to C atoms in other molecules (which are not shown in Fig. 3). In addition, O5 and O4 do not form stable bonding to C2 and C4 and instead bond to C1 and C3 that are located further afterward. In summary, key shock-induced reactions in *c*-axis shock are characterized as massive formation of inter-layer N-N bonds and consequent release of H and O atoms. The mechanochemical initiation of this reaction pathway is reflected in the time progress of the temperature of the N-N in Fig. S5.[19] In addition, the change of electronic structures associated with the inverse Jahn-Teller effect is shown in Fig. S6.[19]

Figures 4(a)–4(d) show time evolution of the number of C-H, C-C, C-N, C-O, N-H, N-N, N-O, O-H, and O-O bonds in *b*-axis and *c*-axis shock. Most remarkable anisotropy appears in the number of produced N-N bonds. This is due to more frequent close encounters of inter-layer N pairs in *c*-axis shock as shown in Fig. 3. Since the inter-layer N-N bond formation is accompanied by the release of H and O atoms, the numbers of N-H and N-O bonds decrease accordingly. In addition, some of the released H and O atoms form H-O bonds. We observed the formation of H_2O molecules in the early stage in *c*-axis shock. Early production of H_2O was also observed by DFTB simulations.[22] Figures 4(e) and 4(f) show time evolution of the number of O atoms that are bonded to H atoms for *b*-axis and *c*-axis shock, respectively. In the figures, OH1, OH2, and OH3 represent O atoms that are only bonded to one, two, and three H atoms, respectively, but are not bonded to other atomic species. While no O-H species are stable over long time for *b*-axis shock, many O atoms are exclusively bonded to H atoms in *c*-axis shock. Breakdown of those O atoms into OH1, OH2, and OH3 species varies in time as shown in Fig. 4(f). This is in accord with the previous simulation study,[22] which also observed OH1, OH2, and OH3 for *c*-axis shock. The drastically different intermediate products (e.g., Figs. 4(e) *vs.* 4(f)) result in different amounts of energy release, hence different temperatures in Fig. 2(a).

We also observe the formation of a number of C-N and C-O bonds in both *b* (Fig. 4(a)) and *c* (Fig. 4(b)) directions. This can be understood as follows: These bonds are easily formed since the electronegativity of C atoms is smaller than those of N and O atoms. On the other hand, the formation of N-N bonds cannot be explained from electronegativity, and instead it has a geometric origin as explained above.

In summary, our QMD simulations revealed a crossover in nanomechanochemical anisotropy in shocked vdW molecular crystal, TATB. Within 10^{-13} s from the passage of shock front, highly sensitive lateral collision produces NO_2 via twisting and bending of nitro-groups mediated by strong *intra-layer* hydrogen bonds. Subsequently, as we transition from heterogeneous to homogeneous mechanochemical regimes around 10^{-12} s, shock normal to layers becomes more sensitive, producing H_2O assisted by *inter-layer* N-N bond formation. Such time-resolved atomistic understanding provides some insight on the relationship between the crystalline geometry, mechanics, and chemistry.

This work was supported by the Office of Naval Research Grant No. N000014-12-1-0555.

[1]J. J. Gilman, Science **274**(5284), 65–65 (1996).
[2]D. A. Davis, A. Hamilton, J. L. Yang, L. D. Cremar, D. Van Gough, S. L. Potisek, M. T. Ong, P. V. Braun, T. J. Martinez, S. R. White, J. S. Moore, and N. R. Sottos, Nature **459**(7243), 68–72 (2009).

[3]P. Balaz, M. Achimovicova, M. Balaz, P. Billik, Z. Cherkezova-Zheleva, J. M. Criado, F. Delogu, E. Dutkova, E. Gaffet, F. J. Gotor, R. Kumar, I. Mitov, T. Rojac, M. Senna, A. Streletskii, and K. Wieczorek-Ciurowa, Chem. Soc. Rev. **42**(18), 7571–7637 (2013).
[4]L. P. Wang, A. Titov, R. McGibbon, F. Liu, V. S. Pande, and T. J. Martinez, Nat. Chem. **6**(12), 1044–1048 (2014).
[5]J. H. Lee, P. E. Loya, J. Lou, and E. L. Thomas, Science **346**(6213), 1092–1096 (2014).
[6]D. W. Brenner, D. H. Robertson, M. L. Elert, and C. T. White, Phys. Rev. Lett. **70**(14), 2174–2177 (1993).
[7]E. J. Reed, M. R. Manaa, L. E. Fried, K. R. Glaesemann, and J. D. Joannopoulos, Nat. Phys. **4**(1), 72–76 (2008).
[8]J. J. Gilman, Mater. Sci. Technol. **22**(4), 430–437 (2006).
[9]M. R. Manaa, Appl. Phys. Lett. **83**(7), 1352–1354 (2003).
[10]Z. F. Wang, Q. X. Li, H. B. Su, X. P. Wang, Q. W. Shi, J. Chen, J. L. Yang, and J. G. Hou, Phys. Rev. B **75**(8), 085424 (2007).
[11]D. Le, A. Kara, E. Schroder, P. Hyldgaard, and T. S. Rahman, J. Phys.: Condens. Matter **24**(42), 424210 (2012).
[12]L. M. Liu, R. Car, A. Selloni, D. M. Dabbs, I. A. Aksay, and R. A. Yetter, J. Am. Chem. Soc. **134**(46), 19011–19016 (2012).
[13]B. B. Averkiev, Z. A. Dreger, and S. Chaudhuri, J. Phys. Chem. A **118**(27), 10002–10010 (2014).
[14]A. K. Geim and I. V. Grigorieva, Nature **499**(7459), 419–425 (2013).
[15]B. Hunt, J. D. Sanchez-Yamagishi, A. F. Young, M. Yankowitz, B. J. LeRoy, K. Watanabe, T. Taniguchi, P. Moon, M. Koshino, P. Jarillo-Herrero, and R. C. Ashoori, Science **340**(6139), 1427–1430 (2013).
[16]S. Dai, Z. Fei, Q. Ma, A. S. Rodin, M. Wagner, A. S. McLeod, M. K. Liu, W. Gannett, W. Regan, K. Watanabe, T. Taniguchi, M. Thiemens, G. Dominguez, A. H. C. Neto, A. Zettl, F. Keilmann, P. Jarillo-Herrero, M. M. Fogler, and D. N. Basov, Science **343**(6175), 1125–1129 (2014).
[17]C. J. Wu, F. H. Ree, and C. S. Yoo, Propell. Explos. Pyrotech. **29**(5), 296–303 (2004).
[18]A. C. Landerville, I. I. Oleynik, and C. T. White, J. Phys. Chem. A **113**(44), 12094–12104 (2009).
[19]See supplementary material at http://dx.doi.org/10.1063/1.4937268 for simulation methods and details.
[20]Y. Li, R. K. Kalia, M. Misawa, A. Nakano, K. Nomura, K. Shimamura, F. Shimojo, and P. Vashishta, "Anisotropic mechanochemistry of energetic van der Waals crystallites: an ab initio nanocollider study" (unpublished).
[21]E. J. Reed, L. E. Fried, and J. D. Joannopoulos, Phys. Rev. Lett. **90**(23), 235503 (2003).
[22]M. R. Manaa, E. J. Reed, L. E. Fried, and N. Goldman, J. Am. Chem. Soc. **131**(15), 5483–5487 (2009).
[23]L. Z. Zhang, S. V. Zybin, A. C. T. van Duin, S. Dasgupta, W. A. Goddard, and E. M. Kober, J. Phys. Chem. A **113**(40), 10619–10640 (2009).
[24]D. E. Taylor, J. Phys. Chem. A **117**(16), 3507–3520 (2013).
[25]Y. Li, R. K. Kalia, A. Nakano, K. Nomura, and P. Vashishta, Appl. Phys. Lett. **105**(20), 204103 (2014).